Journal of the Korean Physical Society, Vol. 77, No. 5, September 2020, pp. 399∼403

Characteristics of a Very High Energy Electron Beam in a Laser Wakefield Accelerator for Cancer Therapy

Kyung Nam Kim, Yonghun Hwangbo, Seok-gy Jeon and Jaehoon Kim*
Electro-Medical Device Research Center, Korea Electrotechnology Research Institute, Ansan 15588, Korea

Soorim Han and Kum Bae Kim
Research Center of Radiological Physics & Engineering, Korea Institute of Radiological and Medical Sciences, Seoul 01812, Korea

(Received 8 January 2020; revised 19 March 2020; accepted 19 March 2020)

A cancer treatment device using a very high energy electron beam has been studied as a new radiation therapy method because of its deep penetration depth, dose characteristics that are better than those of the existing X-ray method, and easy adjustment of the irradiation direction compared to existing equipment. For this treatment, compact high-energy electron accelerators are essential, and a laser wakefield accelerator is a good candidate. In this study, very high energy electrons were accelerated using a laser wakefield accelerator, and the dose characteristics due to these electrons were measured to confirm the possibility of treatment. Electron beam with an energy of 94 MeV were accelerated by using a 16-TW high-power laser, and the dose profile was measured with a tough phantom by using a Gafchromic film. With an 18 nC charge, the peak dose was 120 cGy at a 40 mm depth. The measured dose profile was compared with that obtained using a Monte Carlo simulation with low and high energy electron beams, and the results indicate a quasi-mono-energetic property of the electron beam.

Keywords: Laser wakefield accelerator, Very high energy electron beam, Radiotherapy, Depth dose profile
DOI: 10.3938/jkps.77.399

I. INTRODUCTION

A laser wakefield accelerator (LWFA) [1], that uses the interaction of a femtosecond high-power laser and plasma to accelerate electrons is a possible candidate to make a compact and low-cost high-energy electron accelerator because it can generate 1000 times higher acceleration field than a conventional accelerator. It can also generate an ultra-short-bunch electron beam that can be used for high time-resolution experiments. The characteristics of an electron beam from a LWFA have attracted much interest because of its potential applications on X-ray and betatron radiation sources, and a medical application [2]. Recently, electrons with energies up to 4.2 GeV accelerated by using PW class laser were reported [3,4]. Long-term stability using a LWFA is also being verified [5] for real applications.

Laser wakefield accelerators have two important parameters, one is the injection of the electron into the acceleration phase, and the other is the acceleration of the electron to high energy. Typically, the electrons in the LWFA are injected into the acceleration field by self-injection. The electron beam by self-injection has a high beam charge and narrow energy spread within a 10% bandwidth. However, precise control is required because of nonlinear effects such as self-focusing [6] and self-steepening [7]. In efforts to understand these nonlinear effects, many studies have presented the dependence of tendency to self-focus on laser intensity [8] and the differences in the electron beam according to the injection direction [9]. On the other hand, new injection mechanisms, such as ionization injection [10], colliding laser injection [11], and transition injection [12], have been studied to improve the controllability and stability. The maximum energy of an electron in the LWFA is mainly determined by dephasing, which means that the speed of the electron increases, and the electron goes into the deceleration phase of the acceleration cavity. A non-uniform plasma density was proposed to overcome such effects [13], and the Korea Electrotechnology Research Institute (KERI) has already obtained a 250 MeV electron beam by using a linear-density up-ramp method [14].

Among many applications of the LWFA, a very important application is to build a cancer therapy system because of the energy and the size of the accelerator. Conventional therapy systems based on medical linear accelerators have used photon beam in the energy range

*E-mail: jkim@keri.re.kr

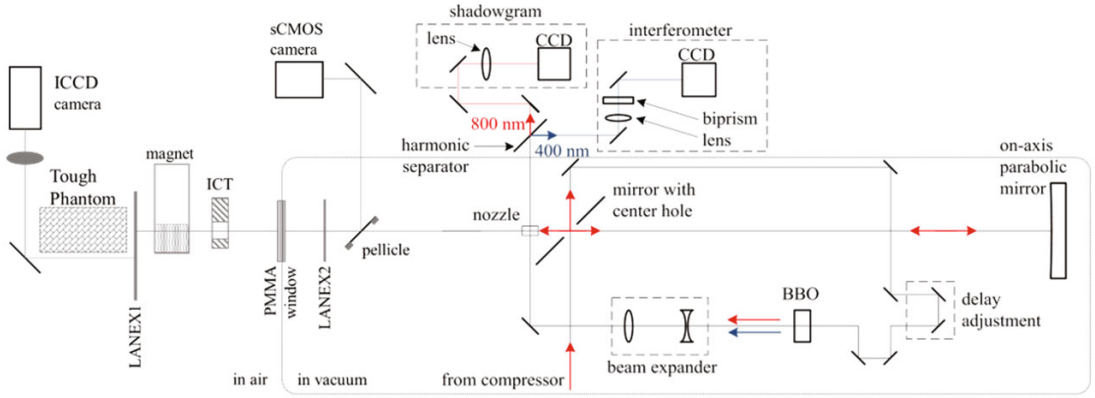

Fig. 1. Schematic of the target chamber for the laser plasma accelerator at the KERI. A parabolic mirror was used to focus the 16-TW laser at the nozzle. The plasma density and profile were measured with a shadowgram and an interferometer. An integrated current transformer (ICT), dipole magnet, and scintillator screens (LANEX) were used for electron diagnostics. For depth-dose measurement, a tough phantom was used after LANEX1. The distance between the nozzle and the tough phantom was 975 mm.

of 6 to 15 MV to remove deep-seated tumors, and electron beams in the energy range of 5 to 20 MeV to remove skin tumors because electrons in this energy range cannot reach deep-seated tumors. However, a very high-energy electron (VHEE) beam with an energy higher than 50 MeV has an exceptional dose deposition and high dose rate compared to photon therapy [15]. The cancer therapy using VHEE beams over 100 MeV has been estimated to be an effective treatment for lung, prostate, brain and neck cancers [16]. In the case of a VHEE beam, the treatment plan becomes simpler because the dose distributions are rarely affected by the irregular structures in the human body, especially air bubbles. Another advantage of a VHEE beam is that the position of the beam can be easily adjusted by using an electric or a magnetic field. For such applications, a compact, high-energy electron accelerator is crucial, and the LWFA is a good candidate. Therefore, the characteristics of the VHEE beam generated in a LWFA and the penetration characteristics in the human body must be clarified.

In this study, physical parameters such as size, charge, energy, and divergence of a VHEE beam generated by a LWFA were measured. Using these VHEE beams, we measured the dosimetric features to verify the feasibility of using a VHEE beam for a cancer therapy system.

II. EXPERIMENTAL SETUP

In order to measure the dosimetric properties of the VHEE beam, we accelerated electrons by using a high-power laser, and we measured the dose characteristics of the electron beam by using an EBT3 film and a tough phantom. Figure 1 shows a schematic of the experiments for the LWFA and the dose measurement. The experiment used a Ti:sapphire laser with peak power 16 TW and a repetition rate of 10 Hz at KERI. This laser uses a typical chirped pulse amplification [17] with a center wavelength of 800 nm. The energy of the laser is 650 mJ at the target, and the pulse duration is 40 fs, which was measured using a single-shot autocorrelator. The compressed laser is reflected by a mirror with a 10 mm diameter hole in the center and focused at the gas target by using an on-axis parabolic mirror with a focal length of 866 mm. The full width at half maximum (FWHM) focal spot size was 18 μm, and the laser beam quality factor, M^2, was 2.0, which was measured using an objective lens with a magnification of 10 and a camera. This measurement shows that the laser intensity is 6.3×10^{18} W/cm^2 and that the normalized vector potential, a_0, is 1.75.

The gas target was generated using a rectangular nozzle and a supersonic gas valve. A gas mixture of 90% helium and 10% nitrogen was used. The density and the fine structure of the plasma generated in the gas target were measured by using an interferometer and shadowgraph. The laser transmitted through the hole in the mirror before the parabolic mirror was converted into a second harmonic wave (SHW) by using a BBO crystal and used as a probe beam of the interferometer. At this time, the 800 nm laser, which was not converted into a SHW was used as a probe beam for the shadowgraph. This structure causes the interferometer and the shadowgraph imaging device to measure the same plasma position at the same time. After the plasma, a harmonic separator was used to separate the probe beams for the interferometer and shadowgraph. The time delay between the probe beam and the main pulse for the LWFA was adjusted by an optical delay. The measured image from the interferometer was converted to the phase change by a using fast Fourier transform [18], and the phase was converted to plasma density by using an Abel inversion [19].

After the nozzle, the characteristics of the electron beam, such as the size, position, energy, and charge,

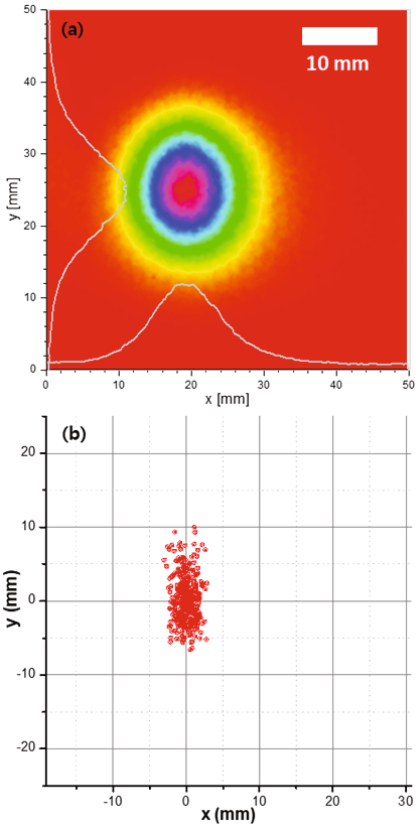

Fig. 2. Electron beam shape and pointing stability measured during the depth-dose measurement. The beam shape was accumulated over 500 shots during the dose measurement as shown in (a). (b) the center position of the electron beam for each exposures, which was measured by using the LANEX 1 screen located at 775 mm from the nozzle.

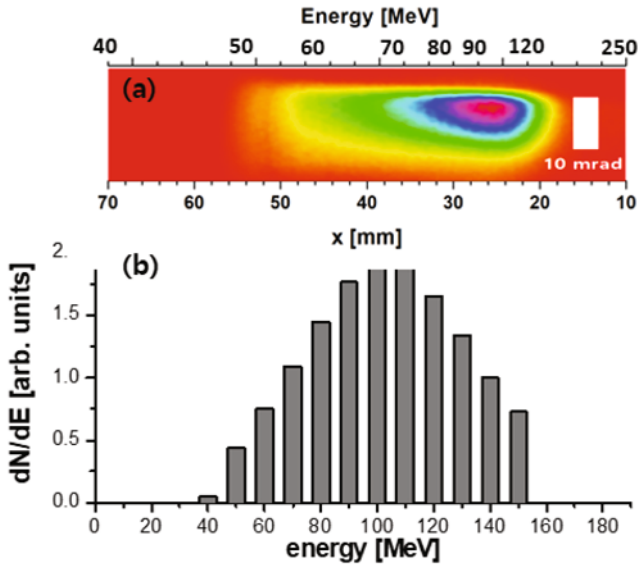

Fig. 3. Results of electron energy measurement. (a) the electron beam image after the magnet accumulated over 80 shots and (b) a histogram of the energy. The energy was measured before and after the dose measurement due to the phantom and magnet interference. A 94 MeV peak energy was measured.

were measured. The electron bunch charge was measured by using an integrated current transformer (Turbo-ICT, Bergoz). The position and the size of the electron beam were measured in two places, front and rear of the dipole magnet used for the energy measurement, by using scintillators (Lanex, Kodak). The two scintillators were installed at 528 mm and 775 mm from the nozzle. The fluorescence images on the scintillators due to the electron beams were acquired using a sCMOS camera (Zyla, Andor Tech.) and an intensified CCD camera (Istar 334, Andor Tech.). Under a magnetic field, the trajectory of the electron is determined by its energy, and the energy of the electron can be measured using this fact. The magnetic field was generated using a dipole magnet. The magnet is 100 mm long and 60 mm wide. The magnetic field at the center is 0.8 T. The magnetic field was precisely measured in two dimensions, and the change in the position of the electron beam under this magnetic field with energy was calculated and converted into energy.

Dose profiles and percent depth dose (PDD) curves were measured by using a tough phantom, consisting of a Gafchromic films (EBT3) and water-equivalent phantoms (ABS plastic, density 1.08 g/cm^3). The distance between the phantom and the nozzle was 975 mm. The tough phantom can measure up to 300 mm deep and 70 mm wide. To measure the dose distribution at the different depth in the phantom, we installed EBT3 films at intervals of 1 mm from the incident position to a 10 mm depth, and thereafter, at 10 mm intervals. When the electron beam is incident on the EBT3 film, darkening that depends on the dose occurs in the film. Thus, each EBT3 film was scanned, and the dose was analyzed using DoseLab (Varian Medical Systems Inc.) to convert the optical density (OD) to a dose. To calibrate the optical density to dose, we used electron beams from a medical linac.

III. RESULTS AND DISCUSSION

To use sufficient charge for dose measurement, we used 500-electron beams to irradiate the phantom. At this time, the position of the electron beam could be measured for each irradiation, but the energy of the electron beam could not be measured. The energy of the electron beam was measured 40 times before and after the dose measurement to reduce the error caused by the change in the electron beam with time. Figure 2 shows the electron beam image over 500 shots and the center position of the beam for each shot, which was measured by using the LANEX 1 screen located at 775 mm from the nozzle. The average electron beam sizes for each shot measured over 500 irradiation were 10.5 ± 1.5 mm and 10.7 ± 1.3

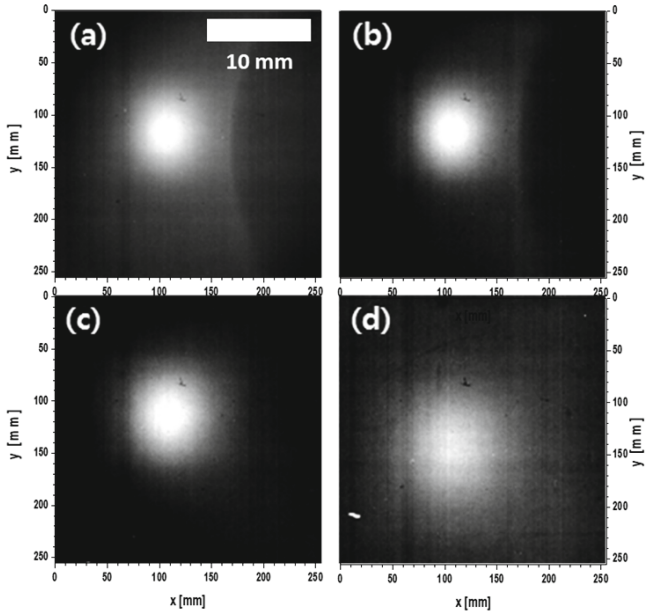

Fig. 4. Scanned images of the EBT3 film at different water equivalent depths: (a) 9.7 mm, (b) 49.9 mm, (c) 105.1 mm, and (d) 149.5 mm.

mm in the horizontal and the vertical directions respectively, and the beam divergences were 5.8 ± 0.8 mrad and 5.9 ± 0.7 mrad. The pointing stabilities of the beams were 4.0 mrad in the vertical direction and 1.4 mrad in the horizontal direction. The total beam sizes, including this pointing stability, were 11.6 mm and 14.0 mm in the horizontal and vertical directions, respectively. This is an improved results compared to the case of pure nitrogen. The pointing stability was 4.2 mrad horizontally and 5.2 mrad vertically when using pure nitrogen gas [20]. The vertical pointing stability was similar, but the horizontal direction was greatly improved. A plasma induced by pure nitrogen has a relatively large number of ionized electrons, which causes continuous electron injection and acceleration. In this case, the number of electrons in the electron bunch is high due to the continuous injection, which increases the beam charge, but makes the beam pointing unstable.

The energy of the electron beam is shown in Fig. 3. The beam dispersed with respect to the energy is shown in Fig. 3(a), and a histogram of the accumulated electron beam energy of the 80 shots used in the energy measurement is shown in Fig. 3(b). The peak energy of each individual measured electron beam energy was the peak energy of 94 MeV with a standard deviation of 80 MeV. Because of the limitation of the magnetic spectrometer, an electron beam with an energy lower than 20 MeV could not be measured.

Figure 4 shows an image of the EBT3 film used for the depth-dose measurement. Each film is measured at depths of 9.7 mm, 49.9 mm, 105.1 mm, and 149.5 mm. The areas obscured in (a) and (b) of Fig. 4 are due to the

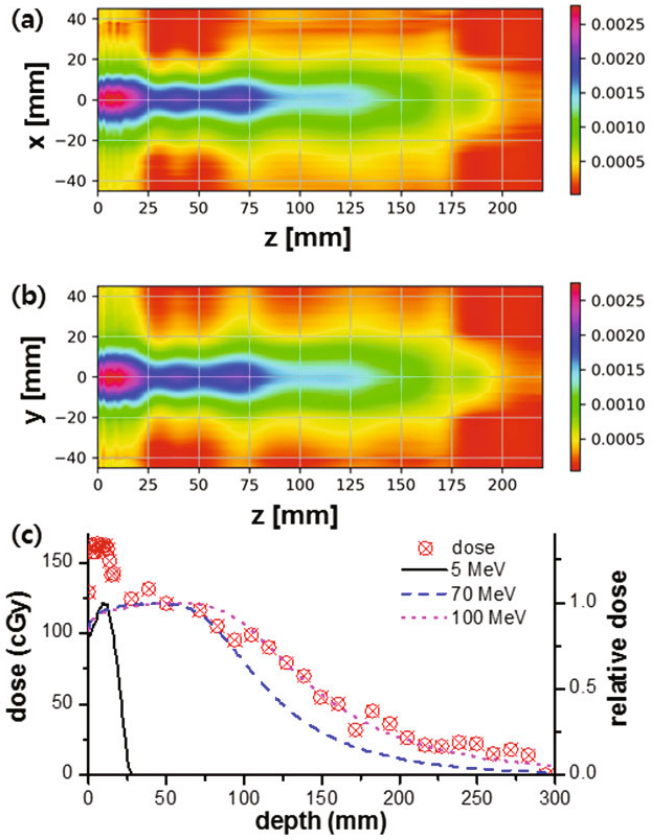

Fig. 5. Depth-dose profile in (a) the horizontal and (b) the vertical directions. (c) Peak dose value as a function of depth with the relative dose profile calculated by using the GEANT4 code. From the measured transverse dose profile, the longitudinal profile was estimated by using interpolation. In (c), the circles are the measured dose, and the line plots are the calculated profiles for different energies.

mirrors used for electron diagnostics. The total charge used for the depth-dose measurement was 18.9 nC over 500 electron beam exposures. After a depth of 25 mm, the maximum dose was 121cGy at 40 mm depth, so the maximum dose per charge was 6.4 cGy/nC.

The dose distribution with depth was measured using the maximum dose at the center of each film. The interpolation method was used to change transverse dose profiles into longitudinal two-dimensional images, and the results are shown in Figs. 5(a) and (b). Figure 5(c) shows the measured depth-dose curve. In the region up to 25 mm from the entrance plane, the dose is quite high, which appears to be the effect of X-rays from the plasma used for acceleration and low-energy electrons.

The depth-dose result was compared with the Monte Carlo calculation for mono-energetic electron beams by using GENANT4 code [21]. Figure 5(c) shows the measured and the calculated depth dose profiles. The circles represent measured results, and the solid and the dashed lines represent the calculated results. From the entrance to a depth of 10 mm, the measured depth dose follows

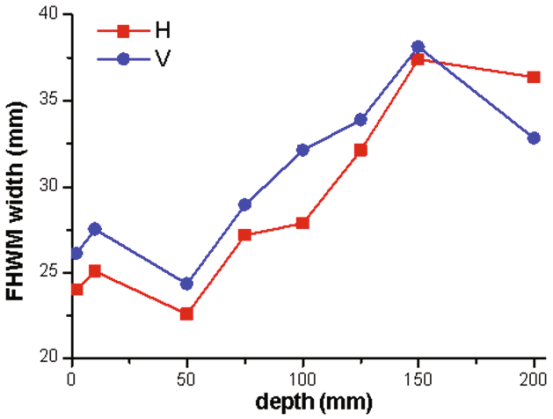

Fig. 6. FHWM of the dose profile at different depths. The dose profile divergence ranged from 50 to 150 mm: H = 138 mrad, V = 130 mrad.

that of low-energy electrons as 5 MeV, and is in good agreement with the dose distribution for 70 MeV in the depth range from 25 mm to 100 mm. After that, the curve follows the depth-dose curve for high-energy electrons. This distribution shows that the electron energy is quasi-mono energetic. Another important point in the depth-dose curve in Fig. 5(c) is the lower entrance dose if we ignore the effects of X-ray and low -energy electrons. This property can reduce the damage to the skin, which is one of the weak points in electron beam therapy using conventional low-energy-electron therapy systems.

The size of the dose distribution measured from each EBT3 film shows different trends depending on the depth, as shown in Fig. 6. The FWHM beam size at the phantom entrance was 24.0 mm in the horizontal direction and 26.1 mm in the vertical direction. At the entrance, a small high-dose profile due to high-energy electrons and a large low-dose profile due to low-energy electrons overlap. When the depth exceeds 50 mm, the low-energy electron beam and low-energy X-rays cannot penetrate, so the beam becomes smaller. The divergences of the dose distribution in the depth range from 50 mm to 150 mm are 138 mrad and 130 mrad in the horizontal and the vertical directions, respectively. Comparing the divergence of the accelerated electron beam with the phantom in the LWFA, we can see that the beam divergence measured in the phantom is very large, but the dose profile is still well collimated.

IV. CONCLUSION

In this study, the physical and the dosimetric properties of very high energy electron beams generated by using a LWFA were measured for VHEE electron therapy. An electron beam with a 94 MeV energy was accelerated in the LWFA. An ionization injection with mixed gas was used to increase stability of the electron beam. This electron beam with a total charge 18 nC over 500 shots was used to measure the depth-dose curve for the VHEE beam. Water equivalent plastic as a tough phantom and EBT3 film were used to measure the dose profile, and a Monte Carlo simulation (GEANT4) was used to calculate the depth-dose curve for mono-energetic high-energy electron beams. The measured depth-dose curve show that the VHEE beam could penetrate deep inside the human body. A comparison of the measured with the calculated data shows a combination of high and low energy electron beams, which is a characteristic of electron beams generated from the LWFA. This energy property must be considered for treatment planning. We hope that these attempts will further increase the applicability of the LWFA's medical devices.

ACKNOWLEDGMENTS

This work was supported by the Creative Allied Project of the National Research Council of Science and Technology (NST, NRF Grant Number: CAP-15-06-ETRI).

REFERENCES

[1] T. Tajima and J. Dawson, Phys. Rev. Lett. **43**, 267 (1979).
[2] K. R Hogstrom and P. R Almond, Phys. Med. Biol. **51**, 455 (2006).
[3] W. P. Leemans *et al.*, Phys. Rev. Lett. **113**, 245002 (2014).
[4] H. T. Kim *et al.*, Nature **7**, 10203 (2017).
[5] J. Faure *et al.*, Nature **444**, 737 (2006).
[6] B. Ritchie, Phys. Rev. E **50**, R687 (1994).
[7] E. Esarey *et al.*, Phys. Rev. Lett. **84**, 3082 (2000).
[8] G. Fibich *et al.*, Opt. Express **13**, 5897 (2005).
[9] S. Corde1 *et al.*, Nat. Commun. **4**, 1501 (2013).
[10] A. Pak *et al.*, Phys. Rev. Lett. **104**, 025003 (2010).
[11] V. Malka *et al.*, Phys. Plasmas **16**, 056703 (2009).
[12] A. Buck *et al.*, Phys. Rev. Lett. **110**, 185006 (2013).
[13] T. Katsouleas, Phys. Rev. A **33**, 2056 (1986)
[14] K. N. Kim, Y. Hwangbo, S-G. Jeon and J. Kim, *2018 IEEE Advanced Accelerator Concepts Workshop (AAC)* (Breckenridge, USA, 2018).
[15] W. P. Levin, H. Kooy, J. S. Loeffler and T. F. DeLaney, Br. J. Cancer **93**, 849 (2005).
[16] E. Schuler *et al.*, Med. Phys. **44**, 2544 (2017).
[17] D. Strickland and G. Mourou, Opt. Commun. **56**, 219 (1985).
[18] J. Kim and G. J. Kim, J. Korean Phys. Soc. **62**, 1662 (2013).
[19] S. Fourmaux *et al.*, Appl. Phys. Lett. **101**, 111106 (2012).
[20] J. Kim, Y. H. Hwangbo and K. N. Kim, Plasma Phys. Control. Fusion **60**, 034008 (2018).
[21] O. Kadri, F. Gharbi and K. Farah, Nucl. Instrum. Methods Phys. Res. B **239**, 391 (2005).